scientific reports

Check for updates

OPEN

# Modification of $TiO_2$ nanotubes by graphene–strontium and cobalt molybdate perovskite for efficient hydrogen evolution reaction in acidic medium

Mariusz Szkoda[1,2]✉, Anna Ilnicka[3], Malgorzata Skorupska[3], Marcin Wysokowski[4] & Jerzy P. Lukaszewicz[3,5]

**Herein, we demonstrate that modification of $TiO_2$ nanotubes with graphene–strontium and cobalt molybdate perovskite can turn them into active electrocatalysts for hydrogen evolution reaction (HER). For this purpose, a simple method of hydrothermal synthesis of perovskites was developed directly on the $TiO_2$ nanotubes substrate. Moreover, the obtained hybrids were also decorated with graphene oxide (GO) during one-step hydrothermal synthesis. The obtained materials were characterized by scanning electron microscopy with energy dispersive X-ray analysis, Raman spectroscopy, and X-ray diffraction analysis. Catalytic properties were verified by electrochemical methods (linear voltammetry, chronopotentiometry). The obtained hybrids were characterized by much better catalytic properties towards hydrogen evolution reaction compared to $TiO_2$ and slightly worse than platinum. The optimized hybrid catalyst (decorated by GO) can drive a cathodic current density of 10 mA $cm^{-2}$ at an overpotential of 121 mV for HER with a small Tafel slope of 90 mV $dec^{-1}$ in 0.2 M $H_2SO_4$.**

Hydrogen evolution reaction (HER) is a crucial reaction in water splitting. It is still required to synthesize inexpensive HER electrocatalysts in a way that is effective, straightforward, and ecologically benign. The design of the appropriate core–shell structure of the catalyst, and controlling thereof shape affect the activity and durability of the catalyst[1]. A three-dimensional structure of the catalyst is beneficial for exposing the surface area, and furnishing the active sites, as well as is propitious to the diffusion and adsorption of hydrogen molecules, expediting the HER process[2,3]. Furthermore, the three-dimensional structure of the catalyst influences oxygen evolution reaction performance[4]. A core–shell hierarchical nanostructure of a catalyst composed of many conductive interconnected networks, provides multiple channels for ionic or electron delivery[5]. The plasma-treated sponge-like nanoalloy exhibits high HER performance due to the exposure of more active and edge sites[6]. Besides the structure of the catalyst, another factor affecting the properties of the catalyst is its doping with, for example, nitrogen heteroatoms[7]. Compare to the well-known and expensive platinum catalyst the $TiO_2$ is widely explored as an alternative catalyst. However, to enhance the electrocatalytic activity of $TiO_2$ different modifications are needed. In some papers, $TiO_2$ has been coupled with metals like nickel[8], ruthenium[9,10], gold[11], cobalt[12], metal oxides like $Co_3O_4$[13], $BiVO_4$[14], or metal–organic frameworks[15]. Very promising materials designed with $TiO_2$ to catalyze the HER are metal sulfides, e.g., $MoS_2$[16–19], $CoS_2$[20], or $WS_2$[21]. Also, hybrid composites with polymers like truxene-based porous organic polymer[22] or poly(aniline)[23], poly(o-phenylenediamine), poly(thiophene), or poly(pyrrole)[24] have proved to be desired candidates to enhance photocatalytic activity of $TiO_2$. Another way to modify the properties of electrocatalyst is doping with non-metals. As described in

[1]Faculty of Chemistry, Department of Chemistry and Technology of Functional Materials, Gdańsk University of Technology, Narutowicza 11/12, 80-233 Gdańsk, Poland. [2]Advanced Materials Center, Gdańsk University of Technology, Narutowicza 11/12, 80-233 Gdańsk, Poland. [3]Faculty of Chemistry, Nicolaus Copernicus University in Torun, Gagarina 7, 87-100 Torun, Poland. [4]Faculty of Chemical Technology, Institute of Chemical Technology and Engineering, Poznan University of Technology, Berdychowo 4, 60-965 Poznań, Poland. [5]Centre for Modern Interdisciplinary Technologies, Nicolaus Copernicus University in Torun, Wilenska 4, 87-100 Torun, Poland. ✉email: mariusz.szkoda1@pg.edu.pl

many papers sulfur-doping, nitrogen-doping, or carbon-doping reduce bandgap of $TiO_2$[25–27]. Another way to improve properties was described by Pandey et al. where in theoretical predictions a hybrid structure of the ionic liquid 1-ethyl-3-methylimidazolium trifluoromethanesulfonate and $(TiO_2)_n$ nanoclusters (with n = 2–12) has been investigated in the pursuit of new catalyst materials for effective HER[28]. Furthermore, hybrids of $TiO_2$ and carbon materials like graphene oxide[13,29] and multi-wall carbon nanotubes[30]. Nanocomposites of graphene oxide with metal–organic framework described in the literature, were also efficient electrocatalyst for hydrogen production via Volmer and Heyrovsky mechanisms[31]. The disadvantage of many solutions is still doping with expensive metals like silver, platinum[29]. Therefore, it is important to find new solutions but without expensive metals and easy to preparation.

In this paper, a novel hybrid materials of $CoMoO_4$, $SrMoO_4$, or their composition $SrMoO_4$ and $CoMoO_4$ deposited on $TiO_2$ nanotubes surface and supported with graphene oxide (GO) were achieved by hydrothermal method. Here, uniform $TiO_2$ nanotubes were used as support to growth $CoMoO_4$ or $SrMoO_4$. The morphology was investigated by scanning electron microscopy (SEM) with energy dispersive X-ray analysis (EDX), Raman spectroscopy, and X-ray diffraction analysis (XRD). These hybrids were subjected as active catalysts for hydrogen evolution reaction in acidic medium. Compared with pristine $TiO_2$ and commercial Pt, the optimal hybrid could attain a current density 10 mA $cm^{-2}$ at a low overpotential of 121 mV with a Tafel slope of 90 mV $dec^{-1}$. In addition, the hybrid displayed better cycling stability and durability.

## Results and discussions

**Physicochemical characterization.** The morphology of the as-prepared samples was characterized by scanning electron microscopy. As shown in Fig. 1a, on the surface of sample $TiO_2/CoMoO_4$ the $TiO_2$ nanotubes are not visible (pure $TiO_2$ nanotubes are presented in Figure S1) because during the hydrothermal process the $CoMoO_4$ particles densely covered $TiO_2$ surface. Intriguingly, each $CoMoO_4$ microspheres (Fig. 1b) is actually a three dimensionally interconnected porous structure and is assembled from numerous nanospheres. For $TiO_2/CoMoO_4$ sample the diameter of $CoMoO_4$ particles ranges from 1 to 2 μm. It can be observed that the particles agglomerate. The surface of $TiO_2/SrMoO_4$ sample (Fig. 1c) clearly demonstrated that the product considered of a large amount of spherical structures covered $TiO_2$ surface and shows the similar morphology to $TiO_2/CoMoO_4$ sample. The diameters of $SrMoO_4$ spheres are about 2 μm. A higher-magnification SEM image (Fig. 1d) reveals that an individual sphere is composed of tens of similar nanosheets. These nanosheets are connected with each other to form a sphere with random orientation. Figure 1e,f illustrate the SEM images for $TiO_2/SrMoO_4/CoMoO_4$ sample with different magnifications. Figure 1f shows the high magnification from which it can be seen that particles deposited on the $TiO_2$ surface do not possess a uniform size and shape. The mean diameters of three-dimensional microspheres are greater and fluctuate between 2 and 4 μm. These nanosheets are connected with each other to form nanosheets-based microstructures with random orientation. Furthermore, the surface of some of the crystals is very smooth. In addition, the energy dispersive X-ray analysis also confirms the $SrMoO_4$ and $CoMoO_4$ structure (Fig. S2).

The morphologies and microstructures of the hybrid materials include of $TiO_2$, $SrMoO_4$ $CoMoO_4$, and GO are present in Fig. 2. These images confirm that applying hydrothermal technology can prepare in one sample three-dimensional structures with different morphology. Figure 2a for $TiO_2/SrMoO_4/GO$ sample indicates the $SrMoO_4$ are randomly distributed on the $TiO_2$ surface. Figure 2b displays that the as-prepared sample $TiO_2/CoMoO_4$ has microstructure with $CoMoO_4$ agglomerated on the surface. It can also be found that these microspheres are consisted of a large number of nanosheets.

The surface morphology of $CoMoO_4$ with GO is comparable to sample without GO. The agglomeration of particles impacts on their size distribution and the average diameter is 1 μm. For sample $TiO_2/SrMoO_4/CoMoO_4/GO$ (Fig. 2c) addition of GO caused to stronger agglomeration of $SrMoO_4$ and $CoMoO_4$ to spherical structures. To visualize the distribution of Co, Mo, Sr, Ti, O, S, and C, energy dispersive X-ray spectroscopy mapping was performed (Fig. S3).

The obtained materials were also structurally characterized by XRD. Figures 3 and 4 shows the XRD pattern of $TiO_2/SrMoO_4$, $TiO_2/CoMoO_4$, $TiO_2/SrMoO_4/CoMoO_4$, $TiO_2/SrMoO_4/GO$, $TiO_2/CoMoO_4/GO$, $TiO_2/SrMoO_4/CoMoO_4/GO$. Some of the $SrMoO_4$ and $CoMoO_4$ peaks overlap with the intense anatase peaks. However, several characteristic peaks from these compounds can be observed, as indicated by the corresponding symbols in Figs. 3 and 4. However, the low intensity of these peaks proves the low crystallinity of $SrMoO_4$ and $CoMoO_4$. Nonetheless, the signature peaks of $SrMoO_4$ at 33.7, 37.1, 38.5, 48.1, 76.3, 77.4, 82.3, 86.8[32–34] and of $CoMoO_4$ at 25.4, 32.4, 36.3, 38.5, 40.2, 45.2, 63.0[35–37] are very prominent in all samples[38,39]. The remaining crystallite phases were indexed as characteristic peaks of anatase and the titanium (Ti) phase acting as $TiO_2$ NT support[40]. The ornamental GO structure peak was observed at 10.5 plane for only a $TiO_2/SrMoO_4/GO$ hybrid. However, the presence of GO can be better characterized by Raman spectroscopy.

Raman spectra of $TiO_2$ nanotubes, $TiO_2/SrMoO_4/CoMoO_4$, and $TiO_2/SrMoO_4/CoMoO_4/GO$ within the frequency range 100–3300 $cm^{-1}$ are shown in Fig. 5. Several bands characteristic for the pure anatase crystalline form were identified in samples of pristine $TiO_2$ and the hybrid materials. However, in the case of a material with added carbon, the anatase peaks are not that pronounced. The bands located at 143, 398, 516, and 640 $cm^{-1}$ are attributed to $E_g(1)$, $B_{1g}$, $A_{1g}$, and $E_g(3)$ active anatase modes, respectively[41,42]. The band at around 326 $cm^{-1}$ is attributed to the symmetric stretching of the Co–O–Mo bond[43]. The peak of around to 300 $cm^{-1}$ corresponds to Sr–O–Mo bond[44]. The band located at 802 $cm^{-1}$ is associated with asymmetric stretching modes of O–Mo–O bond while the band at 904 $cm^{-1}$ corresponds to the symmetric stretching mode of Mo–O bond[45]. On analyzing the Raman bands of modified material by GO, two distinct bands, namely, D and G bands, were obtained at 1347 $cm^{-1}$ and 1580 $cm^{-1}$. The D band is corresponding to disorder carbon while the G band is attributed to $sp^2$ hybridized carbon[46,47]. This confirmed that the graphene component is maintained during the hydrothermal

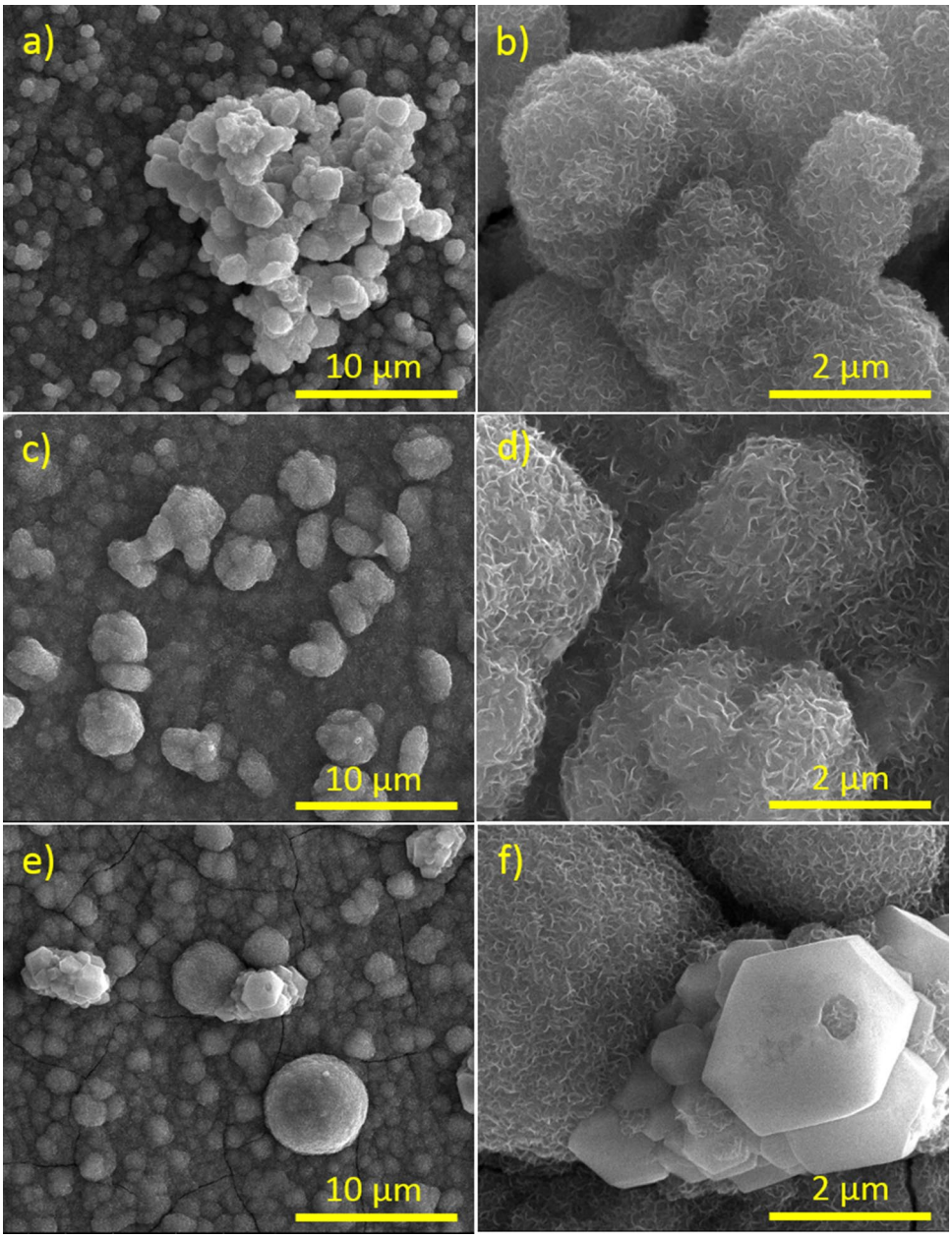


**Figure 1.** SEM images of samples: (**a,b**) $TiO_2/CoMoO_4$, (**c,d**) $TiO_2/SrMoO_4$, (**e,f**) $TiO_2/SrMoO_4/CoMoO_4$.

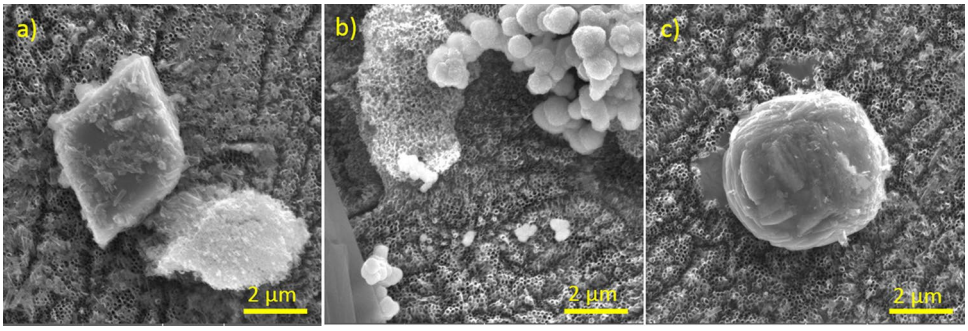


**Figure 2.** SEM images of samples: (**a**) $TiO_2/SrMoO_4/GO$, (**b**) $TiO_2/CoMoO_4/GO$, (**c**) $TiO_2/SrMoO_4/CoMoO_4/GO$.

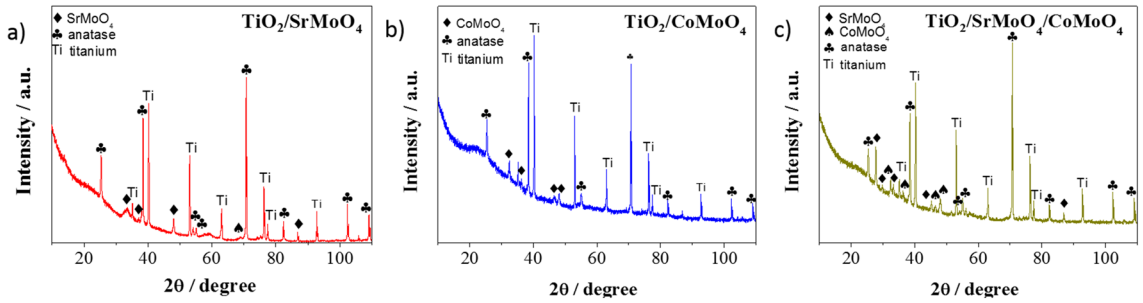


**Figure 3.** X-ray diffraction spectra of samples: (**a**) $TiO_2/SrMoO_4$, (**b**) $TiO_2/CoMoO_4$, (**c**) $TiO_2/SrMoO_4/CoMoO_4$.

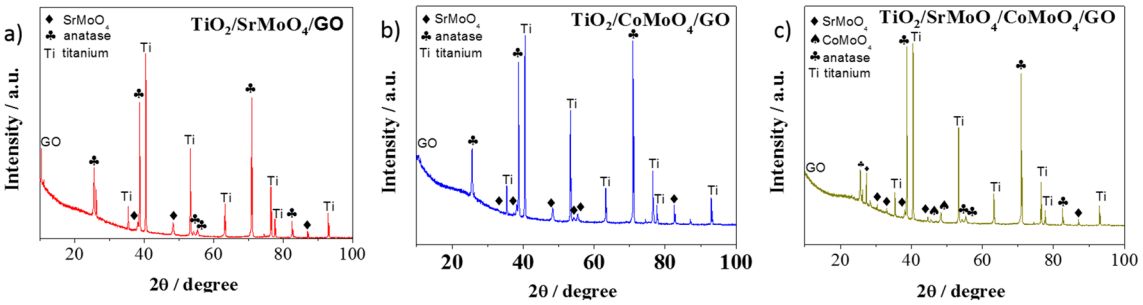


**Figure 4.** X-ray diffraction spectra of samples: (**a**) $TiO_2/SrMoO_4/GO$, (**b**) $TiO_2/CoMoO_4/GO$, (**c**) $TiO_2/SrMoO_4/CoMoO_4/GO$.

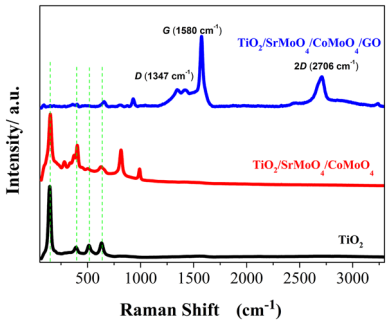


**Figure 5.** Raman spectra of $TiO_2$ nanotubes, $TiO_2/SrMoO_4/CoMoO_4$, and $TiO_2/SrMoO_4/CoMoO_4/GO$.

process. Moreover, the second order of zone boundary phonons or 2D band which is related to the stacking nature of graphene layers was observed at 2706 $cm^{-1}$ for GO[48].

**Electrocatalytic activities for hydrogen evolution.** The catalytic activity of obtained hybrids for hydrogen evolution reaction (HER) was measured in 0.2 M $H_2SO_4$ using three-electrode configuration with a scan rate of 5 mV $s^{-1}$. For comparison, bare $TiO_2$ nanotubes and Pt were also tested. Figure 6a,b give the HER polarization curves of commercial Pt disc, pure $TiO_2$ nanotubes, and the obtained hybrids without and with the addition of carbon.

According to linear sweep voltammograms (LSVs) in Fig. 6a,b, the overpotential values for all electrodes at $j_{HER} = 10$ mA $cm^{-2}$ are summarized in Table 1. The obtained values indicate that a small amount of carbon has a large share in the HER performance of the obtained hybrids. It is worth noting that the η value of $TiO_2/SrMoO_4/CoMoO_4/GO$ is only 29 mV larger than that of pure Pt and comparable to or smaller than those of various transition metal-based electrocatalyst (Table S1).

The electrochemically active surface area (ECSA) was determined to elucidate the effect of composition on HER. The ECSA was estimated using the CV method's double-layer capacitance. For example, Fig. S4 shows the CV for $TiO_2/SrMoO_4/CoMoO_4$ that was performed in the non-Faradaic region at different scanning rates from 0.35 to 0.45 V vs. Ag/AgCl/3 M KCl. For the all obtained electrodes, the charging current at the different scan rates was plotted (Fig. 6c) to obtain the double-layer capacitance from the slope. Can be observed a difference in the double-layer capacitance ($C_{DL}$) between the catalysts depending on the composition. The catalysts modified with graphene oxide have higher $C_{DL}$ values. The ECSA was estimated using the commonly used specific capacity

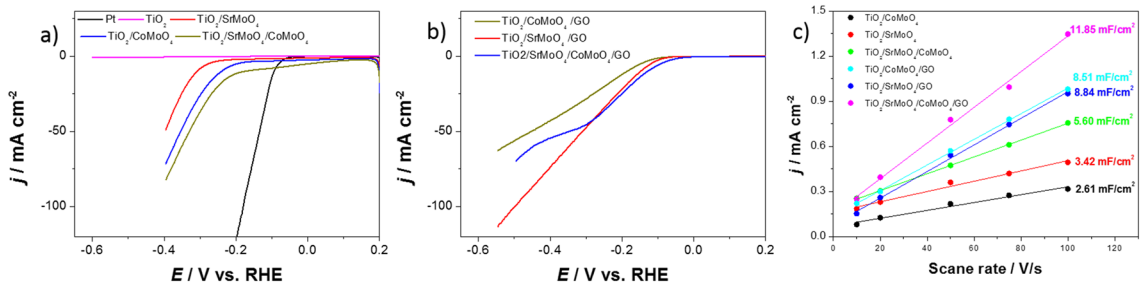


**Figure 6.** LSV curves of obtained catalysts (**a**) without and (**b**) with the addition of carbon. (**c**) Calculated double-layer capacitance ($C_{DL}$) used to estimate the electrochemically active surface area of the obtained catalysts.

| Electrode | Overpotential (mV vs. RHE) to achieve a current density of −10 mA cm$^{-2}$ | Onset potential (mV vs. RHE) | b (mV dec$^{-1}$) | Estimated ECSA (cm$^2$) (0.04 mF cm$^{-2}$) |
|---|---|---|---|---|
| Pt | 92 | −75 | 38 | – |
| $TiO_2$ | Does not achieve | – | 330 | – |
| $TiO_2/SrMoO_4$ | 313 | −275 | 152 | 85.5 |
| $TiO_2/CoMoO_4$ | 242 | −219 | 168 | 65.25 |
| $TiO_2/SrMoO_4/CoMoO_4$ | 167 | −209 | 91 | 140 |
| $TiO_2/SrMoO_4$/GO | 146 | −96 | 62 | 221 |
| $TiO_2/CoMoO_4$/GO | 184 | −121 | 75 | 212.75 |
| $TiO_2/SrMoO_4/CoMoO_4$/GO | 121 | −60 | 90 | 296.25 |

**Table 1.** The HER parameters, Tafel slopes and estimated electrochemically active surface area for the obtained catalysts.

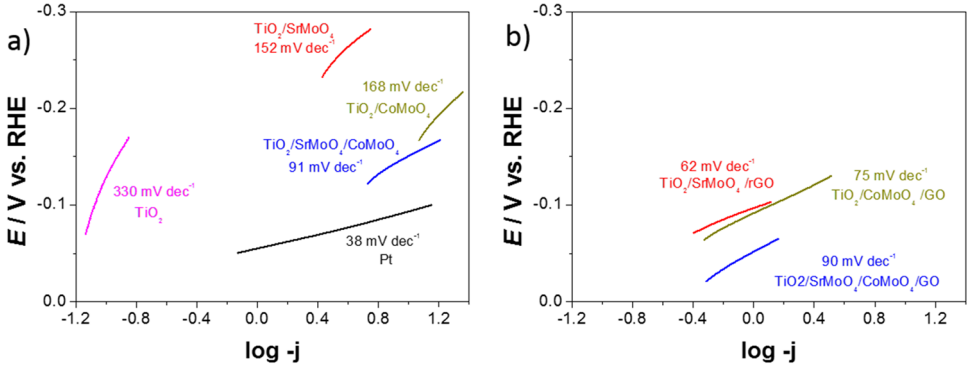


**Figure 7.** The Tafel plots calculated from the corresponding LSV plots for obtained catalysts (**a**) without and (**b**) with the addition of carbon.

of 0.04 mF cm$^{-2}$[49]. Results are summarized in Table 1. The electrochemically active surface area is higher for materials with added carbon, which may impact better catalytic properties toward hydrogen evolution.

Figure S5 shows the electrochemical impedance spectra recorded for obtained catalysts at an open circuit potential. A slightly increasing slope of the curves, in the case of materials modified by carbon, indicates an improving capacitive behavior. Moreover, the small diameter or the absence of a semicircle, in the case of a material with the addition of graphene oxide, indicates the small charge transfer resistance (Rct)[50]. The Rct is associated with the electrocatalytic kinetics at the catalyst/electrolyte interface and gives information about the reaction rate of HER[51]. In summary, the lower the charge transfer resistance, the better the HER kinetics.

Figure 7 presents the Tafel plots. At high overpotentials the HER on the electrodes is kinetically controlled, which can be given by the Tafel equation[52]:

$$\eta = a + b \log j$$

where η (V) means overpotential, $a$ (V) is the cathodic intercept related to the exchange current density, $b$ (V dec$^{-1}$) means the cathodic Tafel slope, and $j$ (A cm$^{-2}$) means catalytic current density. Tafel slope values calculated

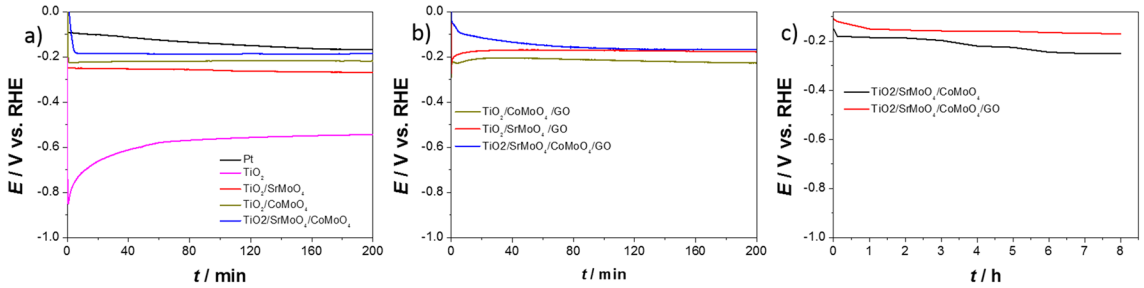


**Figure 8.** Part variations of overvoltage value at a constant current density of 10 mA $cm^{-2}$ with the processing time for (**a**) without and (**b**) with the addition of carbon. (**c**) Chronopotentiometry measurement with the current density of 10 mA $cm^{-2}$ for 8 h for $TiO_2/SrMoO_4/CoMoO_4$ and $TiO_2/SrMoO_4/CoMoO_4/GO$.

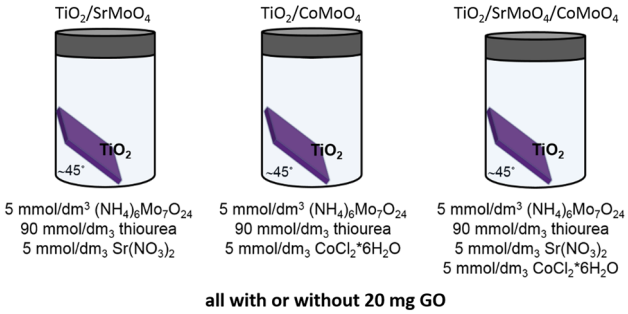


**Figure 9.** Reagents used in the hydrothermal method and their concentration.

from the linear portion of potential vs. logarithmic value of current density deliver useful kinetic metrics of the catalyst[38]. The Tafel slope values were 38, 330, 152, 168, 91, 62, 75, and 90 for Pt, $TiO_2$ nanotubes, $TiO_2/SrMoO_4$, $TiO_2/CoMoO_4$, $TiO_2/SrMoO_4/CoMoO_4$, $TiO_2/SrMoO_4/GO$, $TiO_2/CoMoO_4/GO$, $TiO_2/SrMoO_4/CoMoO_4/GO$, respectively. Concerning as-synthesized electrocatalysts, $TiO_2/SrMoO_4/GO$ showed the lowest Tafel slope value. In this case, the positive effect of the presence of carbon in all hybrids was also observed. The data of Tafel plots along are also tabulated in Table 1.

To examine the long-term stability of obtained electrodes, chronopotentiometric tests were also performed at the fixed current density of 10 mA $cm^{-2}$ (Fig. 8a,b). As can be seen, almost all electrodes show good stability of overpotential with a polarization current of -10 mA $cm^{-2}$. However, in the case of pure $TiO_2$ nanotubes the overpotential had shifted from 842 to 541 mV by the end of 200 min. In other cases, the overpotential oscillates between 261 and 140 mV.

In order to verify the validity of the modification with graphene oxide, an even longer stability test (8 h) was performed for the best materials without and with the addition of carbon. As shown in Fig. 8c, the overpotential of $TiO_2/SrMoO_4/CoMoO_4$ decreased from −152 to −251 mV during 8 h, indicating lower stability compared with the same material but with the addition of carbon. The results demonstrate that adding GO during synthesis can greatly enhance its stability and electrocatalytic performance for hydrogen evolution in an acidic solution. According to the literature[53–55], in carbon–metal hybrid materials, transition metals exhibit remarkable catalytic abilities, while the carbon material provides better conductivity, stability and greater surface area. In addition, interactions between carbon and metallic materials can change the properties of the whole hybrid, contributing to the formation of new sites with increased catalytic activity.

## Materials and methods

**$TiO_2$ nanotubes preparation.** $TiO_2$ nanotubes were prepared by one-step anodization of titanium film according to a previously optimized procedure[56]. First, the titanium sheets, placed in a mixture of acetone and isopropanol (1:1 ratio), were cleaned using ultrasound for 20 min. Anodization was carried out in a two-electrode system in which both the anode and cathode were titanium sheets. Electrodes were placed in 50 $cm^3$ water:glycol mixture (volume ratio 1:19) about 2 cm separated from each other. The electrolyte contained 0.27 M ammonium fluoride and 1 M phosphoric acid (V). The anodization process was carried out for 2 h at a constant voltage of 40 V. The nanotubes obtained on the titanium foil were washed with a solution of 100 µl HF in 50 $cm^3$ water (to remove inorganic impurities), followed by distilled water. In the last step, the obtained material was calcined at 450 °C for 2 h. As a result, $TiO_2$ NT were transformed from amorphous to crystalline form.

**Synthesis of hybrids.** The layer of $SrMnO_4$, $CoMoO_4$ and $SrMoO_4/CoMoO_4$, respectively, was deposited on $TiO_2$ nanotubes by hydrothermal method. Appropriate amounts of each component of the reaction mixture (Fig. 9) were dissolved in 15 mL of deionized water to form a clear solution. Hybrids were made with or without 20 mg of GO added to the reaction mixture.

After that, the as-prepared fresh solution and $TiO_2$ nanotubes plate were transferred into a Teflon-lined stainless autoclave (30 mL), which was then tightly sealed and left in an oven at 220 °C for 7 h. After the autoclave cooled down to room temperature, the $TiO_2$ nanotube plate with black layer was taken out and washed with deionized water several times to remove unstable products, which was then dried in a vacuum oven at 60 °C.

**Solid state physics techniques.** A MIRA3 scanning electron microscope (SEM) (Tescan, Czech Republic) was used to assess the surface. The crystalline phases were characterized by X-ray diffractometer (Philips X"Pert with detector X'Celerator Scientific). Raman spectra were recorded with a Raman spectrometer (Senterra, Bruker Optik) with a green laser (532 nm) used as the excitation source.

**Electrochemical characterization.** A three-electrode cell consisting of a working electrode, Pt as a counter electrode and Ag/AgCl (in 3 M KCl) as a reference electrode has been employed. 0.2 M $H_2SO_4$ solution has been used as electrolyte. All the electrochemical measurements have been performed using potentiostat/galvanostat (BioLogic VSP 2078) at room temperature. Unless otherwise specified, all potentials measured were referenced to the reversible hydrogen electrode (RHE) using the following equation: E (RHE) = E (Ag/AgCl) + 0.21 + 0.059 pH. Linear sweep voltammograms were obtained with a scan rate of 1 mV $s^{-1}$. Tafel plots were derived from the corresponding LSV curves. The long-term stability was tested by a chronopotentiometric technique at a −10 mA $cm^{-2}$ current density. The electrochemically active surface area (ECSA) was estimated through the cyclic voltammetry method. Under a non-Faradaic region, a series of CV scans were performed at different scan rates (10, 20, 50, 75, 100 mV $s^{-1}$). The double-layer capacitance ($C_{DL}$) was found by obtaining the slope of the linear fit. The ECSA of obtained electrodes was determined on the basis of the equation: $ECSA = \frac{C_{DL}}{C_s}$, where Cs is the specific capacitance. The $C_s$ used for our calculations was 0.040 mF $cm^{-2}$—value commonly used for metals[49,57]. Moreover, EIS was performed for two of the best materials in a frequency range between 20 kHz and 1 Hz with a voltage amplitude of 10 mV at an open circuit potential.

## Conclusions

An efficient hybrid catalyst in the form of $TiO_2$ nanotubes with $CoMoO_4$, $SrMoO_4$, and graphene oxide on their surface was proposed in this research. The strategy of creating active centers by modification of $TiO_2$ with carbon and perovskite-type metal oxide in one synthesis step may pave the way toward the synthesis of cheap, efficient, and stable catalysts. As a result, $TiO_2/SrMoO_4/CoMoO_4$/GO hybrid was proved to be an efficient and durable HER electrocatalyst in acidic medium. The optimized catalyst only required a low overpotential of 120 mV at 10 mA $cm^{-2}$ with a Tafel slope of 90 mV $dec^{-1}$, superior to results of pristine $TiO_2$. The high HER activity and excellent durability of $TiO_2/SrMoO_4/CoMoO_4$/GO hybrid make it a promising alternative to commercial Pt-based HER catalyst.

## Data availability

The datasets generated and/or analysed during the current study are available in the BRIDGE OF KNOWLEDGE repository (https://mostwiedzy.pl/en/open-research-data/x-ray-diffraction-spectra-of-modification-of-tio2-nanotubes-by-graphene-strontium-and-cobalt-molybda,1128104009119681-0).

Received: 29 September 2022; Accepted: 27 December 2022
Published online: 30 December 2022

## References

1. Chuyen Phan, T., Nguyen, V.-T., Choi, H.-S. & Kim, H. Highly efficient and durable electrochemical hydrogen evolution reaction based on composition/shape controlled CuTi@Pt core-shell nanotubes in acidic media. *Appl. Surface Sci.* **605**, 154331. https://doi.org/10.1016/j.apsusc.2022.154331 (2022).
2. Zhang, X. *et al.* Defect-rich MnxOy complex Fe–Ni sulfide heterogeneous electrocatalyst for a highly efficient hydrogen evolution reaction. *J. Power Sources* **540**, 231664 (2022).
3. Nguyen, V.-T. *et al.* In situ engineering of Pd nanosponge armored with graphene dots using Br– toward high-performance and stable electrocatalyst for the hydrogen evolution reaction. *ACS Appl. Mater. Interfaces* **12**, 15500–15506. https://doi.org/10.1021/acsami.9b13735 (2020).
4. Yan, Q. *et al.* In situ formed edge-rich $Ni_3S_2$–NiOOH heterojunctions for oxygen evolution reaction. *J. Electrochem. Soc.* **169**, 054532 (2022).
5. Nguyen, V.-T., Nguyen, V.-C., Phan, T. C., Choi, H.-S. & Kim, H. Boosting electrocatalytic oxygen evolution activity by in-situ growth of hierarchical vertically-erected $Ni(OH)_2$ nanosheets on Ag nanowires. *Int. J. Hydrogen Energy* **47**, 31614–31623 (2022).
6. Nguyen, N.-A. *et al.* Plasma-treated sponge-like NiAu nanoalloy for enhancing electrocatalytic performance in hydrogen evolution reaction. *Catal. Today* **337**, 90–96. https://doi.org/10.1016/j.cattod.2019.03.019 (2019).
7. Chai, L. *et al.* Bottom-up synthesis of MOF-derived hollow N-doped carbon materials for enhanced ORR performance. *Carbon* **146**, 248–256. https://doi.org/10.1016/j.carbon.2019.02.006 (2019).
8. Franceschini, E. A., Gomez, M. J. & Lacconi, G. I. One step synthesis of high efficiency nickel/mesoporous $TiO_2$ hybrid catalyst for hydrogen evolution reaction. *J. Energy Chem.* **29**, 79–87 (2019).
9. Wei, Z. *et al.* Oxygen-deficient $TiO_2$ and carbon coupling synergistically boost the activity of Ru nanoparticles for the alkaline hydrogen evolution reaction. *J. Mater. Chem. A* **9**, 10160–10168 (2021).
10. Wang, K. *et al.* Crystalline Ru0.33Se nanoparticles-decorated $TiO_2$ nanotube arrays for enhanced hydrogen evolution reaction. *Small* **14**, 1802132 (2018).
11. Zabelin, D. *et al.* Design of hybrid Au grating/$TiO_2$ structure for NIR enhanced photo-electrochemical water splitting. *Chem. Eng. J.* **443**, 136440 (2022).
12. Feng, J. X. *et al.* Efficient hydrogen evolution electrocatalysis using cobalt nanotubes decorated with titanium dioxide nanodots. *Angew. Chem. Int. Ed.* **56**, 2960–2964 (2017).
13. Noor, S., Sajjad, S., Leghari, S. A. K., Flox, C. & Kallio, T. Efficient electrochemical hydrogen evolution reaction and solar activity via bi-functional GO/$Co_3O_4$–$TiO_2$ nano hybrid structure. *Int. J. Hydrogen Energy* **45**, 17410–17421 (2020).

14. Sadeghzadeh-Attar, A. Boosting the photocatalytic ability of hybrid $BiVO_4$–$TiO_2$ heterostructure nanocomposites for $H_2$ production by reduced graphene oxide (rGO). *J. Taiwan Inst. Chem. Eng.* **111**, 325–336 (2020).
15. Yan, B., Liu, D., Feng, X., Shao, M. & Zhang, Y. Ru species supported on MOF-derived N-doped $TiO_2$/C hybrids as efficient electrocatalytic/photocatalytic hydrogen evolution reaction catalysts. *Adv. Funct. Mater.* **30**, 2003007 (2020).
16. Song, X., Chen, G., Guan, L., Zhang, H. & Tao, J. Interfacial engineering of $MoS_2$/$TiO_2$ hybrids for enhanced electrocatalytic hydrogen evolution reaction. *Appl. Phys. Exp.* **9**, 095801 (2016).
17. Tao, J. *et al.* Well-patterned Au nanodots on $MoS_2$/$TiO_2$ hybrids for enhanced hydrogen evolution activity. *Electrochim. Acta* **283**, 419–427 (2018).
18. Wang, W. *et al.* Edge-enriched ultrathin $MoS_2$ embedded yolk-shell $TiO_2$ with boosted charge transfer for superior photocatalytic $H_2$ evolution. *Adv. Funct. Mater.* **29**, 1901958 (2019).
19. Cheng, C. *et al.* Enhanced visible light catalytic activity of $MoS_2$/$TiO_2$/Ti photocathode by hybrid-junction. *Appl. Catal. B* **237**, 416–423 (2018).
20. Ganesan, P., Sivanantham, A. & Shanmugam, S. $CoS_2$–$TiO_2$ hybrid nanostructures: Efficient and durable bifunctional electrocatalysts for alkaline electrolyte membrane water electrolyzers. *J. Mater. Chem. A* **6**, 1075–1085 (2018).
21. Liu, S. *et al.* Ultrathin $WS_2$ nanosheets vertically aligned on $TiO_2$ nanobelts as efficient alkaline hydrogen evolution electrocatalyst. *Int. J. Hydrogen Energy* **45**, 1697–1705 (2020).
22. Valverde-González, A. *et al.* Understanding charge transfer mechanism on effective truxene-based porous polymers–$TiO_2$ hybrid photocatalysts for hydrogen evolution. *ACS Appl. Energy Mater.* **3**, 4411–4420 (2020).
23. Chen, B. *et al.* Enhanced light-driven hydrogen-production activity induced by accelerated interfacial charge transfer in donor–acceptor conjugated polymers/$TiO_2$ hybrid. *Chem. A. Eur. J.* **25**, 3362–3368 (2019).
24. Reddy, K. R., Hassan, M. & Gomes, V. G. Hybrid nanostructures based on titanium dioxide for enhanced photocatalysis. *Appl. Catal. A* **489**, 1–16 (2015).
25. Yuan, W. *et al.* Laminated hybrid junction of sulfur-doped $TiO_2$ and a carbon substrate derived from $Ti_3C_2$ MXenes: Toward highly visible light-driven photocatalytic hydrogen evolution. *Adv. Sci.* **5**, 1700870 (2018).
26. Basavarajappa, P. S. *et al.* Recent progress in metal-doped $TiO_2$, non-metal doped/codoped $TiO_2$ and $TiO_2$ nanostructured hybrids for enhanced photocatalysis. *Int. J. Hydrogen Energy* **45**, 7764–7778 (2020).
27. Liu, M. *et al.* Regulation of hydrogen evolution performance of titanium oxide–carbon composites at high current density with a Ti–O hybrid orbital. *Carbon Energy* (2022).
28. Pandey, D. K., Kagdada, H. L., Materny, A. & Singh, D. K. Hybrid structure of ionic liquid and $TiO_2$ nanoclusters for efficient hydrogen evolution reaction. *J. Phys. Chem. A* **125**, 2653–2665 (2021).
29. Wang, P., Han, L., Zhu, C., Zhai, Y. & Dong, S. Aqueous-phase synthesis of Ag-$TiO_2$-reduced graphene oxide and Pt-$TiO_2$-reduced graphene oxide hybrid nanostructures and their catalytic properties. *Nano Res.* **4**, 1153–1162 (2011).
30. Tian, L., Ye, L., Deng, K. & Zan, L. $TiO_2$/carbon nanotube hybrid nanostructures: Solvothermal synthesis and their visible light photocatalytic activity. *J. Solid State Chem.* **184**, 1465–1471 (2011).
31. Makhafola, M. D. *et al.* Palladinized graphene oxide-MOF induced coupling of Volmer and Heyrovsky mechanisms, for the amplification of the electrocatalytic efficiency of hydrogen evolution reaction. *Sci. Rep.* **11**, 17219. https://doi.org/10.1038/s41598-021-96536-9 (2021).
32. Hosseinpour-Mashkani, S. M., Sobhani-Nasab, A. & Mehrzad, M. Controlling the synthesis $SrMoO_4$ nanostructures and investigation its photocatalyst application. *J. Mater. Sci. Mater. Electron.* **27**, 5758–5763 (2016).
33. Liu, Y.-F., Dai, S.-H., Lu, Y.-N. & Min, H.-H. Microwave heating synthesis and luminescence property of $Eu^{3+}$ doped $SrMoO_4$ micro-octahedrons. *Powder Technol.* **221**, 412–418 (2012).
34. Chun, F. *et al.* Preparation and luminescent properties of self-organized broccoli-like $SrMoO_4$: $Pr^{3+}$ superparticles. *J. Lumin.* **190**, 69–75 (2017).
35. Mai, L.-Q. *et al.* Hierarchical $MnMoO_4$/$CoMoO_4$ heterostructured nanowires with enhanced supercapacitor performance. *Nat. Commun.* **2**, 1–5 (2011).
36. Nti, F., Anang, D. A. & Han, J. I. Facilely synthesized $NiMoO_4$/$CoMoO_4$ nanorods as electrode material for high performance supercapacitor. *J. Alloy Compd.* **742**, 342–350 (2018).
37. Ramkumar, R. & Minakshi, M. Fabrication of ultrathin $CoMoO_4$ nanosheets modified with chitosan and their improved performance in energy storage device. *Dalton Trans.* **44**, 6158–6168 (2015).
38. Kareem, A., Kunhiraman, A. K. & Maiyalagan, T. Hydrogen evolution reaction catalyzed by microstructured $SrMoO_4$ decorated on three-dimensional nanostructured rGO/f-MWCNT in acidic medium. *Ionics* **26**, 5055–5064 (2020).
39. Zhang, Y. *et al.* New $NiMoO_4$/$CoMoO_4$ composite electrodes for enhanced performance supercapacitors. *Ionics* **26**, 3579–3590 (2020).
40. Li, H., Tang, N., Yang, H., Leng, X. & Zou, J. Interface feature characterization and Schottky interfacial layer confirmation of $TiO_2$ nanotube array film. *Appl. Surf. Sci.* **355**, 849–860 (2015).
41. Gupta, S. M. & Tripathi, M. A review of $TiO_2$ nanoparticles. *Chin. Sci. Bull.* **56**, 1639–1657 (2011).
42. Trzciński, K., Szkoda, M., Siuzdak, K., Sawczak, M. & Lisowska-Oleksiak, A. Electrochemical and photoelectrochemical characterization of photoanodes based on titania nanotubes modified by a $BiVO_4$ thin film and gold nanoparticles. *Electrochim. Acta* **222**, 421–428 (2016).
43. Ahmed, J., Ubaidullah, M., Ahmad, T., Alhokbany, N. & Alshehri, S. M. Synthesis of graphite oxide/cobalt molybdenum oxide hybrid nanosheets for enhanced electrochemical performance in supercapacitors and the oxygen evolution reaction. *ChemElectroChem* **6**, 2524–2530 (2019).
44. Muralidharan, M., Anbarasu, V., Elaya Perumal, A. & Sivakumar, K. Enhanced ferromagnetism in Cr doped $SrMoO_4$ scheelite structured compounds. *J. Mater. Sci. Mater. Electron.* **27**, 2545–2556 (2016).
45. Liu, F. *et al.* Multi-dimensional CuO nanorods supported $CoMoO_4$ nanosheets heterostructure as binder free and high stable electrode for supercapacitor. *J. Mater. Sci. Mater. Electron.* **29**, 10353–10361 (2018).
46. Zhou, G. *et al.* Oxygen bridges between NiO nanosheets and graphene for improvement of lithium storage. *ACS Nano* **6**, 3214–3223 (2012).
47. Li, N. *et al.* Battery performance and photocatalytic activity of mesoporous anatase $TiO_2$ nanospheres/graphene composites by template-free self-assembly. *Adv. Funct. Mater.* **21**, 1717–1722 (2011).
48. How, G. T. S., Pandikumar, A., Ming, H. N. & Ngee, L. H. Highly exposed 001 facets of titanium dioxide modified with reduced graphene oxide for dopamine sensing. *Sci. Rep.* **4**, 1–8 (2014).
49. Connor, P., Schuch, J., Kaiser, B. & Jaegermann, W. The determination of electrochemical active surface area and specific capacity revisited for the system MnOx as an oxygen evolution catalyst. *Z. Phys. Chem.* **234**, 979–994 (2020).
50. Lu, C. *et al.* Nitrogen-doped $Ti_3C_2$ MXene: mechanism investigation and electrochemical analysis. *Adv. Funct. Mater.* **30**, 2000852 (2020).
51. Li, R. *et al.* Nitrogen doped $MoS_2$ nanosheets synthesized via a low-temperature process as electrocatalysts with enhanced activity for hydrogen evolution reaction. *J. Power Sources* **356**, 133–139 (2017).
52. Herraiz-Cardona, I., Ortega, E., Vázquez-Gómez, L. & Pérez-Herranz, V. Double-template fabrication of three-dimensional porous nickel electrodes for hydrogen evolution reaction. *Int. J. Hydrogen Energy* **37**, 2147–2156 (2012).

53. Zhang, W. *et al.* Recent development of transition metal doped carbon materials derived from biomass for hydrogen evolution reaction. *Int. J. Hydrogen Energy* (2022).
54. Murthy, A. P., Madhavan, J. & Murugan, K. Recent advances in hydrogen evolution reaction catalysts on carbon/carbon-based supports in acid media. *J. Power Sources* **398**, 9–26 (2018).
55. Zhou, W. *et al.* Recent developments of carbon-based electrocatalysts for hydrogen evolution reaction. *Nano Energy* **28**, 29–43 (2016).
56. Szkoda, M. *et al.* Electrodes consisting of PEDOT modified by Prussian Blue analogues deposited onto titania nanotubes—Their highly improved capacitance. *Solid State Ionics* **302**, 197–201 (2017).
57. McCrory, C. C. *et al.* Benchmarking hydrogen evolving reaction and oxygen evolving reaction electrocatalysts for solar water splitting devices. *J. Am. Chem. Soc.* **137**, 4347–4357 (2015).

## Acknowledgements

The research leading to these results has received funding from the Norway Grants 2014-2021 via the National Centre for Research and Development. This work was carried out as a result of the research project no. NOR/SGS/IL-HYDROGEN/0202/2020-00.

## Author contributions

M.Sz.: Conceptualization, Methodology, Investigation, Formal analysis, Visualization, Writing—original draf, Writing—review & editing, Supervision. A.I.: Methodology, Investigation, Formal analysis, Visualization, Writing—original draf, Writing—review & editing, Project administration, Funding acquisition. M.Sk.: Investigation, Formal analysis. M.W.: Investigation, Formal analysis, Technical help. J.P.L.: Conceptualization, Writing—review & editing.

## Competing interests

The authors declare no competing interests.

## Additional information

**Supplementary Information** The online version contains supplementary material available at https://doi.org/10.1038/s41598-022-27143-5.

**Correspondence** and requests for materials should be addressed to M.S.

**Reprints and permissions information** is available at www.nature.com/reprints.

**Publisher's note** Springer Nature remains neutral with regard to jurisdictional claims in published maps and institutional affiliations.